

SURROGATE-ASSISTED HIERARCHICAL OPTIMIZATION METHOD FOR VARIABLE SWEEP FLIGHT VEHICLE TRAJECTORY

Nianhui Ye¹, Teng Long^{1,2}, Bo Fu³ & Renhe Shi^{1,4}

¹School of Aerospace Engineering, Beijing Institute of Technology, Beijing, P.R. China
 ²Key Laboratory of Dynamics and Control of Flight Vehicle, Ministry of Education
 ³Xi'an Modern Control Technology Research Institute, Xi'an, People's Republic of China
 ⁴Beijing Institute of Technology Chongqing Innovation Center, Chongqing, China

Abstract

Morphing flight vehicles can adaptively change the configuration to achieve favorable aerodynamic performance for different flight conditions, which has attracted much attention in recent years. As the most crucial procedure, the trajectory design generally determines the morphing flight vehicle performance. To sufficiently improve the flight range, a surrogate-assisted hierarchical optimization method is developed for the variable sweep flight vehicle trajectory, which consists of inner and external optimization processes. In the inner optimization process, the trajectory is optimized by the pseudospectral method to maximize the flight range, where the angle of attack and sweep angle change rates are selected as the control variables. Compared with the fixed wing, the variable sweep wing can extend the total range by 6.79%. In the external optimization process, the boundary states of different trajectory phases (i.e., initial trajectory angle of each phase, terminal trajectory angle and velocity) are optimized to further increase the flight range. Considering the time-consuming inner optimization process, a Kriging surrogate-assisted differential evolution method is adopted to execute the external optimization efficiently and effectively. After the external optimization, the total range can be further increased by 15.86% compared with the initial morphing flight vehicle trajectory.

Keywords: Morphing flight vehicle; trajectory; pseudospectral method; surrogate; optimization

1. Introduction

Morphing flight vehicle, capable of adaptively changing the configuration, to achieve favorable aerodynamic performance in real time for different flight conditions and task requirement [1]. According to the morphing modes, the crucial morphing approaches can be categorized as variable wing and airfoil [2, 3], deflectable nose [4, 5], variable inlet [6], and active flow control [7]. Compared with the other morphing approaches, the variable wing and airfoil approach is much more efficient for performance improvement and easily to be realized [8, 9].

Since 1930s, a considerable amount of flight vechicles with morphing wing have been conducted by the United States and the Soviet Union. At that time, the variable-sweep angle and variable span are the most ultized approaches to improve the performance under different flight conditions. For instances, F-14, Su-17, and MiG-23 aircraft ultized variable-sweep wings to adapt themselves in both subsonic and supersonic conditions [8]. Meanwhile, variable-span wings are integrated with MAK-10 and MAK-123 to enhance the flight range [10]. To qualitatively and quantitatively analyze the merits of morphing wings, some research have been carried out. As for the swept wings, Vos et al. [11] point out the mechanism of postponing the strong shock waves and drag divergence as for the variable-sweep wing. Dai et al. [2] propose a variable sweep wing configuration for a waverider, which performance is then investigated under subsonic, supersonic, and hypersonic flight conditions. The results show that the large sweep angle can reduce the drag coefficient in all the studied conditions. Additionally, Bae et al. [12] conduct a detailed analysis on the aerodynamic and static aeroelastic characteristics of a variable-span morphing wing. The results show that with the increment of span, both the lift coefficient and wing-root bending moment increased considerably.

The aforementioned literature mainly focuses on evaluating the lift and drag characteristics caused by morphing wings, while the favorable effect for the trajectory is rarely discussed. During the preliminary design, it is crucial to determine the morphing rule, i.e., the change of the morphing part in different states or times. In this way, the benefit of the morphing wing can be quantitatively assessed and the preliminary design of the morphing flight vehicle [1, 13]. To obtain the best morphing rules, the trajectory optimization methods are preferred to solve such an optimal control problem [14]. The most two common approaches for addressing this problem are direct and indirect methods. The indirect methods attempt to satisfy the necessary conditions of optimality, which convergence is sensitive to the initial guess [14]. The direct methods can be categorized as the shooting method, the evolutionary optimization method, and the collocation method [15]. Among these methods, the collocation method is widely used due to its convergence merit. For instance, Dai et al. [16] define the sweep angle of a waverider as the control variables and utilized the Gauss pseudo-spectral method to maximize the flight range. The optimied results reveal that the variable sweep wing can lead to a 13% increment of downrange distance. Moreover, some scholars integrate the evolutionary optimization method with the collocation method to improve the trajectory optimization performance. Gong et al. [17] develop a bi-level global optimization method for a two-stage reusable flight vehicle, where the sub-level optimization is conducted for each trajectory phase, while the system-level optimiztaion is for coordinating the joint points. Similarly, Wu et al. [18] propose a hybrid particle swarm optimization (PSO)-gauss pseudo method (GPM) for re-entry trajectory optimization of hypersonic vehicle. In this way, GPM works in the inner loop to solve the reentry trajectory optimization problem, while PSO is performed in the outer loop to optimize the initial guess.

However, the time consuming inner loop for the trajectory optimization has greatly limited the evolutionary optimization employment in the outer loop. To address the challenge of computational burden problems, surrogate base optimization methods have attracted great attentions over the past decade [19]. Inspired by those method, the time consuming inner loop can be approximated by the surrogate, which can then provied efficient prediction [20]. Thus, it is a new endeavor to develop a surrogate-assisted hierarchical optimization method for the flight vehicle trajectory.

The remainder of this paper is organized as follows. The preliminary design of the morphing flight vehicle, including the scheme trajectory and aerodynamic coefficient, is given in Section 2. Section 3 presents the inner optimization process, which focuses on optimizing the control variables. In section 4, the external optimization process is performed to refine the boundary states of different trajectory phases. Finally, the conclusions and future works are summarized in Section 5.

2. Preliminary Design for Morphing Flight Vehicle

2.1 Scheme Trajectory and Configuration Design

The scheme trajectory of the morphing flight vehicle is first given as shown in Figure 1, which consists of boosting, aerial cruising, and diving phases. In the boosting phase, the flight vehicle is launched from the land and climbs to a high altitude to gain a broader sight. The flight vehicle then descends to a low altitude and cruises for a certain range. After the cruising phase, the flight vehicle pitches down and arrives at the target location. The total flight range is set as 10~30km.

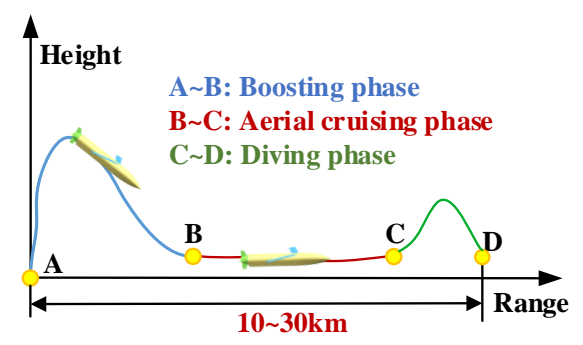


Figure 1 – Scheme trajectory of morphing flight vehicle

Considering several different phases in the entire trajectory, variable sweep wing is employed to provide sufficient lift or reduce drag, as shown in Figure 2 [21]. According to Ref. [21], the overall length of the body is set as 5.33m. The chord and span of the variable-sweep wing are set as 0.40m

and 3.40m, respectively. The wings are generally deployed with a small sweep angle to provide sufficient lift during the aerial cruising phase. When the velocity is small, the sweep angle is increased to reduce the drag.

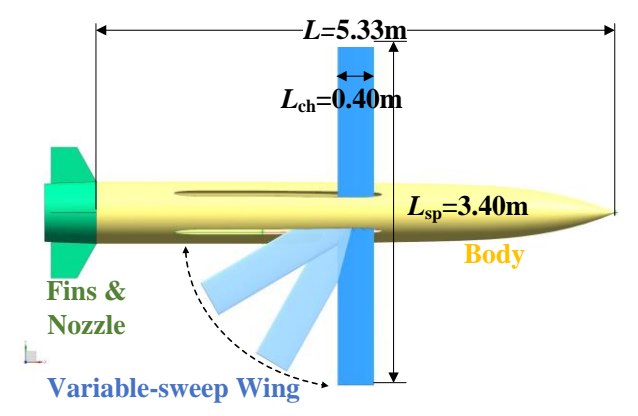


Figure 2 – Morphing flight vehicle configuration [21]

The solid rocket motor with an end-burning strategy is utilized to provide an approximately fix thrust during working time. The detailed parameters of the propulsion system are detailed in the following table.

Table 1 – Parameters of propulsion system

Parameter	Unit	Value	Parameter	Unit	Value					
Thrust in A~B phase	N	800	Mass flow in A~B phase	kg/s	0.40					
Thrust in B~D phase	Ν	400	Mass flow in B~D phase	kg/s	0.20					
Working time of A~B phase	S	30	Specific impulse of SRM	N⋅s/kg	2000.00					
Working time of B~D phase	s	60	Initial total mass	kg	300.0					

2.2 Aerodynamic Modeling

In this paper, the computation fluid dynamics (CFD) is utilized for the lift and drag calculation. Since several special-shaped parts are involved, unstructured grids are applied to generate the mesh model. Furthermore, a local grid refinement is performed to accurately capture the flow field around the flight vehicle, which is shown in Figure 3.

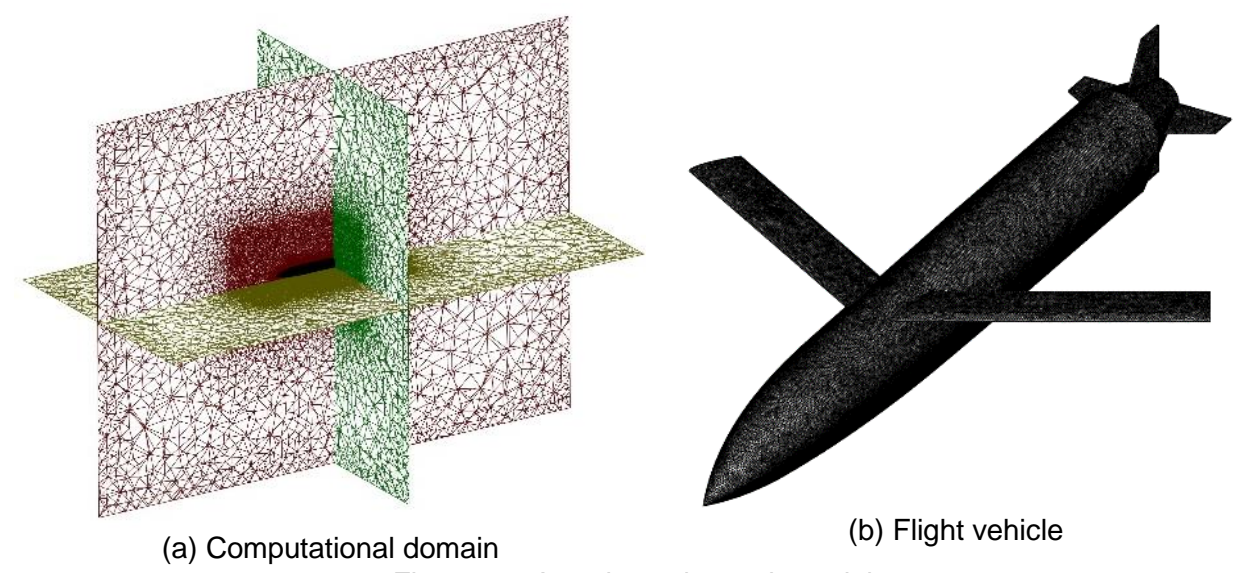
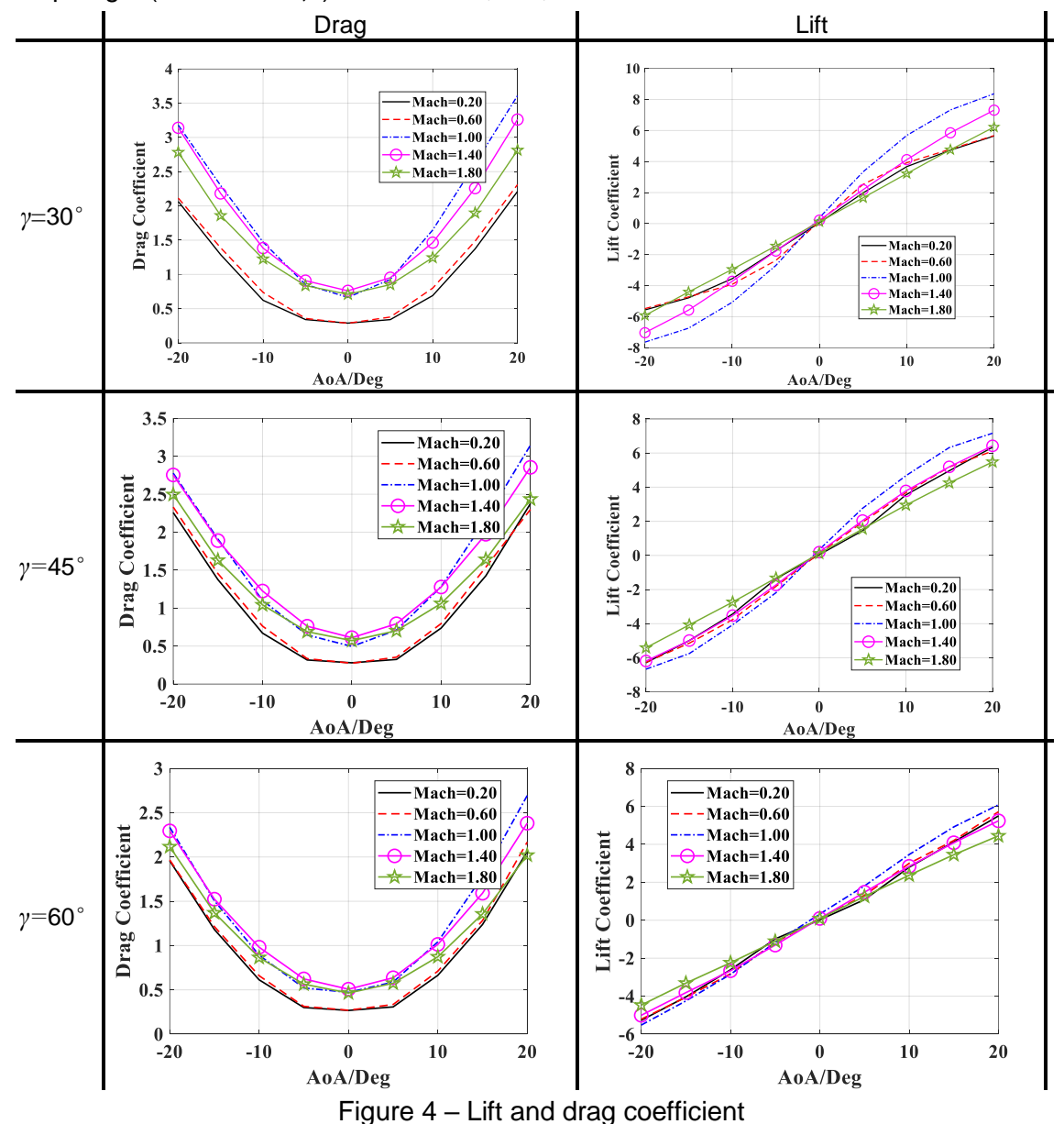


Figure 3 – Aerodynamic mesh model

Based on the mesh model, the Navier–Stokes equation incorporates with Spalart–Allmaras turbulence model to obtain the aerodynamic performance. The flight condition of the aerial trajectory covers Mach number from 0.2 to 1.8 and angle of attack (AoA) from -20° to 20°. The results of the

aerodynamic coefficients are illustrated in Figure 4, where the reference area is set as 0.0985 m² and the sweep angle (denoted as γ) is set as 30°, 45°, and 60°.



From Figure 4, it can be found that with the increment of the sweep angle, the drag and lift coefficients gradually decrease, where various aerodynamic performances can be obtained. Thus, the sweep angle is required to be refined to achieve better performance for different flight conditions.

2.3 Hierarchical Optimization Framework

To sufficiently improve the flight range of the morphing flight vehicle, a surrogate-assisted hierarchical optimization method is proposed in this paper, as shown in Figure 5. The overall optimization procedure is divided into two parts, i.e., inner and external optimization processes.

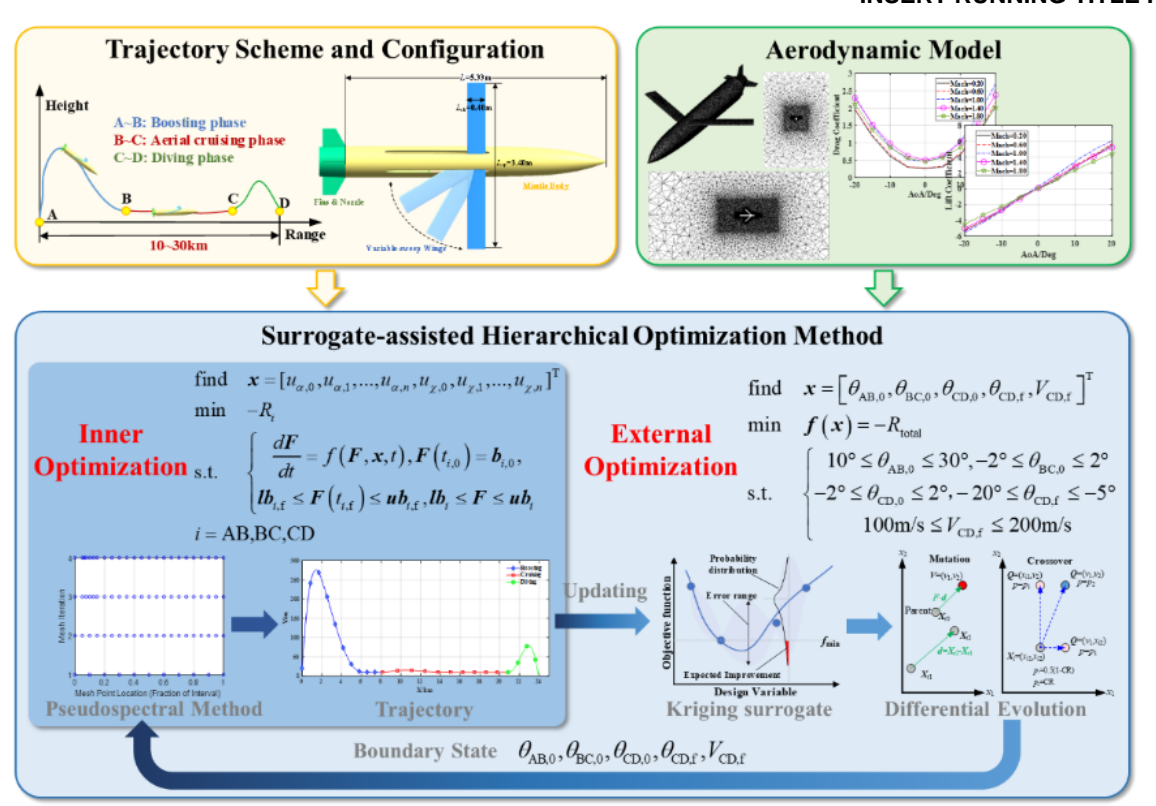


Figure 5 – Hierarchical optimization process

The inner optimization process aims to optimize several control variables, i.e., angle of attack and sweep angle change rates, based on the pseudospectral method. Additionally, the external optimization process focus on refining the boundary states of different trajectory phases to further improve the flight range. The details on the inner and external optimization processes are elaborated in Section 3 and Section 4, respectively.

3. Inner Optimization Process

3.1 Dynamic Equation

In this paper, the dynamic equation of the morphing flight vehicle is established based on the trajectory coordinate systems, as formulated as

$$\frac{dV}{dt} = (P\cos\alpha - X - mg\sin\theta)/m$$

$$\frac{d\theta}{dt} = (P\sin\alpha + Y - mg\cos\theta)/(mV)$$

$$\frac{dx}{dt} = V\cos\theta$$

$$\frac{dy}{dt} = V\sin\theta$$

$$\frac{dm}{dt} = -m_{sa}$$

$$\frac{d\alpha}{dt} = u_{\alpha}$$

$$\frac{d\gamma}{dt} = u_{\gamma}$$
(1)

where $\left[V,\theta,x,y,m,\alpha,\gamma\right]^{\mathrm{T}}$ is the state variable, i.e., velocity, trajectory angle, horizontal displacement, vertical displacement, mass, AoA, and sweep angle, respectively; P, X, and Y denote the thrust, aerodynamic drag and lift forces; u_{α} and u_{γ} are the changing rates of AoA and sweep angle.

3.2 Inner Optimization Problem Definition

In this paper, $u_{\alpha} \in [-2,2]^{\circ}/s$ and $u_{\gamma} \in [-2,2]^{\circ}/s$ are selected as the control variables, which are optimized by Radau Pseudospectral method. The objective functions of all the phases are defined to maximize the flight range. The inner optimization problem can be formulated as

find
$$\mathbf{x} = [u_{\alpha,0}, u_{\alpha,1}, ..., u_{\alpha,n}, u_{\chi,0}, u_{\chi,1}, ..., u_{\chi,n}]^{\mathrm{T}}$$

min $-R_i$
s.t.
$$\begin{cases} \frac{d\mathbf{F}}{dt} = f(\mathbf{F}, \mathbf{x}, t), \mathbf{F}(t_{i,0}) = \mathbf{b}_{i,0}, \\ l\mathbf{b}_{i,f} \leq \mathbf{F}(t_{i,f}) \leq u\mathbf{b}_{i,f}, l\mathbf{b}_i \leq \mathbf{F} \leq u\mathbf{b}_i \end{cases}$$

$$i = \Delta \mathbf{B} \mathbf{B} \mathbf{C} \mathbf{C} \mathbf{D}$$
(2)

where R_i is the range of each phase; $F(t_{i,0})$ and $F(t_{i,f})$ are the initial and final state variables in each phase; $b_{i,0}$ is the values of the initial state variables; $b_{i,f}$ and $b_{i,f}$ are the low and upper boundaries of the final state variables; b_i and b_i are the low and upper boundaries of the state variables; f(F,x,t) is the dynamic equation. The values of the aforementioned items are summarized in Table 2.

Table 2 - Inner optimization problem definition

Table 2 – Inner optimization problem definition							
Phase	Item	Value					
Boosting phase	$oldsymbol{b}_{ ext{AB},0}$	[300m/s, 20°, 0, 20m, 300kg, 0, 45°]					
	$\emph{lb}_{ ext{AB,f}}$	[100m/s,0,1km,10m,0,-2°,30°]					
	$m{ub}_{ ext{AB,f}}$	[600m/s,0,50km,15m,300kg,2°,60°]					
	$\emph{lb}_{\scriptscriptstyle ext{AB}}$	$[100 \text{m/s}, -40^{\circ}, 0, 10 \text{m}, 0, -20^{\circ}, 30^{\circ}]$					
	$m{ub}_{ ext{AB}}$	[600m/s,40°,50km,300m,300kg,20°,60°]					
Cruising phase	$oldsymbol{b}_{ ext{BC},0}$	$m{F}\left(t_{\mathrm{AB,f}} ight)$					
	$\emph{lb}_{ ext{BC,f}}$	[100m/s,3°,1km,10m,0,0,30°]					
	$m{u}m{b}_{ m BC,f}$	[600m/s,3°,50km,15m,300kg,10°]					
	$\emph{lb}_{ ext{BC}}$	[100m/s, -3°, 1km, 10m, 0, -20°, 30°]					
	$oldsymbol{u}oldsymbol{b}_{ ext{BC}}$	[600m/s,3°,50km,15m,300kg,20°]					
Diving phase	$oldsymbol{b}_{ ext{CD},0}$	$m{F}\left(t_{ ext{BC,f}} ight)$					
	$\emph{lb}_{ ext{CD,f}}$	[150m/s, -15°, 1km, 0.5m, 0, 0, 30°]					
	$\pmb{u}\pmb{b}_{ ext{CD,f}}$	[150m/s,-15°,50km,0.5m,300kg,0,60°]					
	$\emph{lb}_{ ext{CD}}$	[100m/s, -40°, 1km, 0.5m, 0, -20°, 30°]					
	$\pmb{u}\pmb{b}_{ ext{CD}}$	[600m/s,40°,50km,500m,300kg,20°,60°]					

3.3 Radau Pseudospectral Method

The problem in Eq. (2) is conducted via Radau Pseudospectral method (RPM), where the dynamic equations can be simplified as

$$\dot{\boldsymbol{x}}(t) = f(t, \boldsymbol{x}(t), \boldsymbol{u}(t)), \quad t \in [t_0, t_f]
\boldsymbol{x} = [V, \theta, x, y, m, \alpha, \gamma]^{\mathrm{T}}
\boldsymbol{u} = [u_{\alpha}, u_{\gamma}]^{\mathrm{T}}$$
(3)

In RPM, the time is normalized to [-1, 1]. Then, N Legendre-Gauss-Radau (LGR) allocation points are generated, where the state and control variables are approximated by interpolation polynomial as [22]

$$\begin{cases} \boldsymbol{x}(\tau) \approx \boldsymbol{X}(\tau) = \sum_{i=1}^{N} L_{i}(\tau) \boldsymbol{X}_{i}(\tau), & L_{i}(\tau) = \prod_{j=1, j \neq i}^{N} \frac{\tau - \tau_{j}}{\tau_{i} - \tau_{j}} \\ \boldsymbol{u}(\tau) \approx \boldsymbol{U}(\tau) = \sum_{i=1}^{N} \tilde{L}_{i}(\tau) U_{i}(\tau), & \tilde{L}_{i}(\tau) = \prod_{j=1, j \neq i}^{N-1} \frac{\tau - \tau_{j}}{\tau_{i} - \tau_{j}} \end{cases}$$

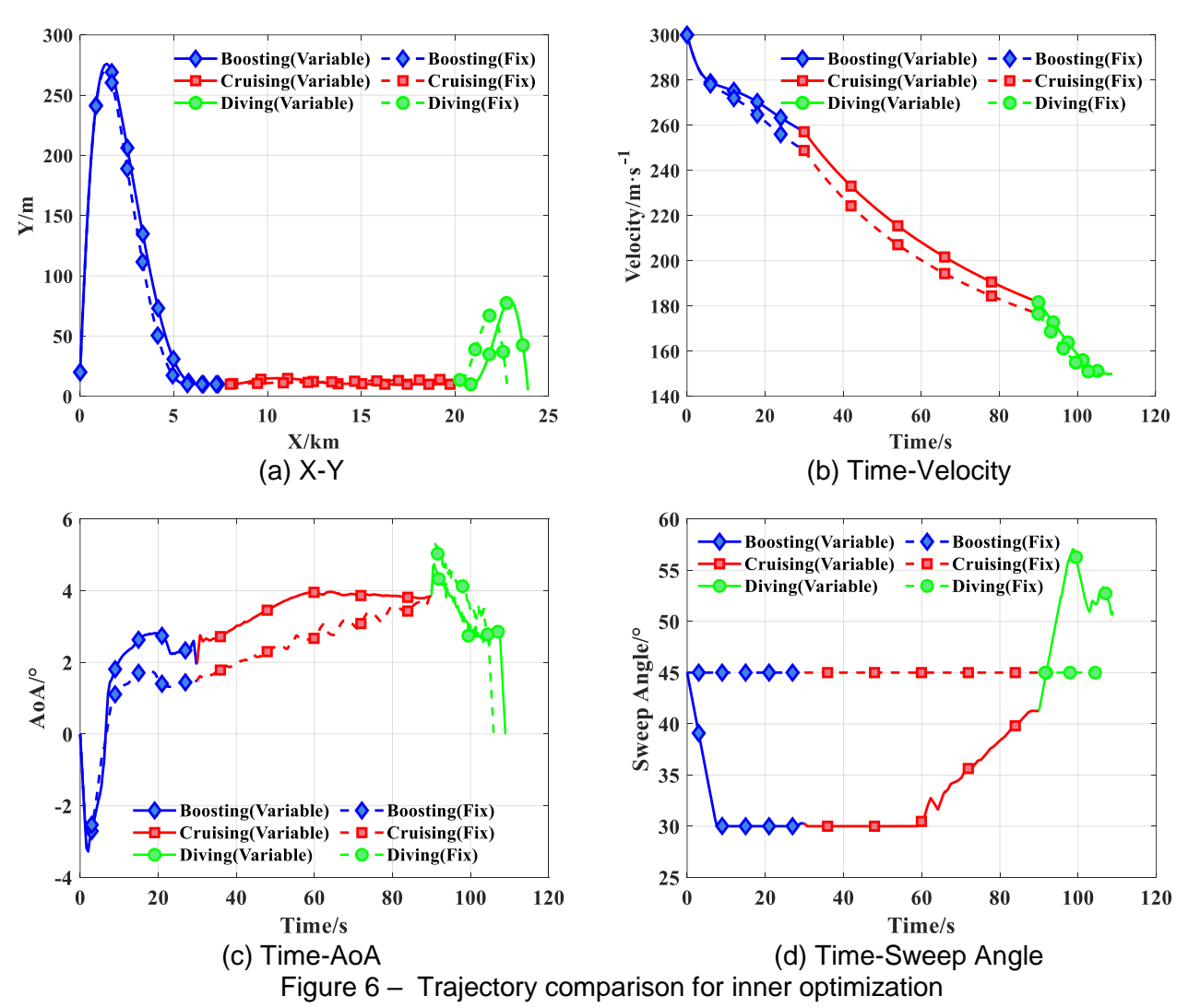
$$(4)$$

where $(\tau_1, \tau_2, ..., \tau_N)$ are the roots of the sum of the N-1 & N -order Legendre polynomials; $X_i(\tau)$ and $U_i(\tau)$ is the approximation of the state and control variables at τ_i . Thus, the problem can be addressed by searching the proper variables as

$$\boldsymbol{X}^* = \left[X \left(\tau_1 \right), ..., X \left(\tau_N \right), U \left(\tau_1 \right), ..., U \left(\tau_N \right), t_f \right]$$
 (5)

3.4 Inner Optimization Result and Analysis

After solving by RPM, the aerial trajectories with the fixed wing (γ = 45°) and variable sweep wing are summarized in Figure 6. The results demonstrate that the total ranges of trajectories with the fixed and variable sweep wings are 22.8078km and 24.0565km, respectively. The variable sweep wing can improve the flight range by 6.79%, where the proper sweep angle is utilized for different phases. For instances, the sweep angle maintains a small value when t < 60s . This is because the small sweep angle can bring a large lift force for cruising. Meanwhile, the sweep angle gradually increases when t > 60s to reduce the drag force during the diving phase, which leads to the satisfaction of the final velocity constraint.



4. External Optimization Process

4.1 External Optimization Problem Definition

Note that the RPM focuses on optimizing the control variables of the trajectory, which fails to determine the best boundary states for different phases. Thus, the external optimization mathematic model is established to maximize the total range R_{total} via refining the boundary states. The design variables consist of the initial trajectory angle of the boosting, cruising, and diving phases (denoted as $\theta_{\text{AB},0}$, $\theta_{\text{BC},0}$, $\theta_{\text{CD},0}$), final trajectory angle of the diving phase (denoted as $\theta_{\text{CD},f}$), and the final velocity (denoted as $V_{\text{CD},f}$).

find
$$\mathbf{x} = \begin{bmatrix} \theta_{AB,0}, \theta_{BC,0}, \theta_{CD,0}, \theta_{CD,f}, V_{CD,f} \end{bmatrix}^T$$

min $\mathbf{f}(\mathbf{x}) = -R_{total}$ (6)
s.t.
$$\begin{cases} 10^{\circ} \le \theta_{AB,0} \le 30^{\circ}, -2^{\circ} \le \theta_{BC,0} \le 2^{\circ} \\ -2^{\circ} \le \theta_{CD,0} \le 2^{\circ}, -20^{\circ} \le \theta_{CD,f} \le -5^{\circ} \\ 100 \text{m/s} \le V_{CD,f} \le 200 \text{m/s} \end{cases}$$

Considering the time-consuming inner process, the external optimization problem is regarded as an expensive optimization problem. Therefore, a Kriging surrogate-assisted differential evolution method (KRG-DE) is employed to improve the total range within the limited computational resources. KRG-DE is introduced in the following subsection.

4.2 Kriging Surrogate-Assisted Differential Evolution

In KRG-DE, the time-consuming inner trajectory optimization process is approximated by Kriging to. In this way, the external optimization efficiency can be improved. The optimization procedure of KRG-DE can be divided into two phase, i.e., global exploration and local exploitation. In the global exploration, differential evolutionary operators are invoked to generate candidate sample points, which are then elected based on the expected improvement by Kriging. In additional, a radial basis function is constructed and combined with a local optimizer to accelerate the convergence speed.

Step 1. Define the external trajectory optimization problem, including the objective, constraints, and design variables. Meanwhile, set up the maximum number of function evaluations $N_{\rm fe,max}$ for KRG-DE.

Step 2. Utilize maximin Latin hypercube sampling method to generate initial sample points [23]. The true responses of those sample points, i.e., the total flight range, are calculated based on the inner trajectory optimization. The sample points and their responses are then used to initialize the database store.

Step 3. The parent population X_g is selected from the database based on the feasibility rule [24].

Step 4. Several differential evolutionary operators are executed to generate the offspring population, as expressed as

$$u_i = x_{r1} + F \cdot (x_{r2} - x_{r3}) \tag{7}$$

$$\mathbf{v}_{i} = \begin{bmatrix} v_{i,1}, v_{i,2}, ..., v_{i,n_{v}} \end{bmatrix}$$

$$v_{i,j} = \begin{cases} u_{i,j} & \text{if } \text{rand}(0,1) \le p_{\text{CR}} \\ x_{i,j} & \text{otherwise} \end{cases}$$
(8)

In the equations above, F and p_{CR} are the scaling factor and crossover probability, i.e., 0.8 and 0.9, according to Ref. [25]; u_i and v_i are mutation and offspring individuals; x_{r1} , x_{r2} , and x_{r3} are the randomly selected parent individuals from X_g . After the execution of Eqs. (7) and (8), the candidate sample points of size N_p can be obtained as $V_g = [v_1, v_2, ..., v_{NP}]$.

Step 5. A kriging is trained based on all the samples in the database. Then, a global infill sample point

 $\mathbf{\textit{x}}_{\mathrm{gi}}$ is elected from V_{g} according to expected improvement as formulated as

$$E(\mathbf{x}) = \begin{cases} \left(y_{\min} - \hat{f}_{KRG}(\mathbf{x})\right) \Phi\left(\frac{y_{\min} - \hat{f}_{KRG}(\mathbf{x})}{\hat{s}_{f}(\mathbf{x})}\right) + \hat{s}_{f} \phi\left(\frac{y_{\min} - \hat{f}_{KRG}(\mathbf{x})}{\hat{s}_{f}(\mathbf{x})}\right) & \text{if } \hat{s}_{f} > 0\\ 0 & \text{if } \hat{s}_{f} = 0 \end{cases}$$

$$(9)$$

where y_{\min} is the best objective value in the database; \hat{f}_{KRG} and \hat{s}_f are the predicted objective and corresponding variance via kriging.

Step 6. A local infill sample point x_{ij} is obtained by solving the following optimization problem

find
$$\mathbf{x} = \left[\theta_{AB,0}, \theta_{BC,0}, \theta_{CD,0}, \theta_{CD,f}, V_{CD,f}\right]^T$$

min $\hat{f}_{RBF}(\mathbf{x})$
s.t.
$$\begin{cases}
10^{\circ} \le \theta_{AB,0} \le 30^{\circ}, -2^{\circ} \le \theta_{BC,0} \le 2^{\circ} \\
-2^{\circ} \le \theta_{CD,0} \le 2^{\circ}, -20^{\circ} \le \theta_{CD,f} \le -5^{\circ} \\
100\text{m/s} \le V_{CD,f} \le 200\text{m/s}
\end{cases}$$
(10)

where \hat{f}_{RBF} is an approximate model of the flight range using radial basis function.

Step 7. Calculate the real responses for the global and local infill sample points. Then, store these sample points and their responses into the database.

Step 8. If $N_{\rm fe,max}$ is reached, KRG-DE terminates and outputs the best samples in database. Otherwise, go back to step 3.

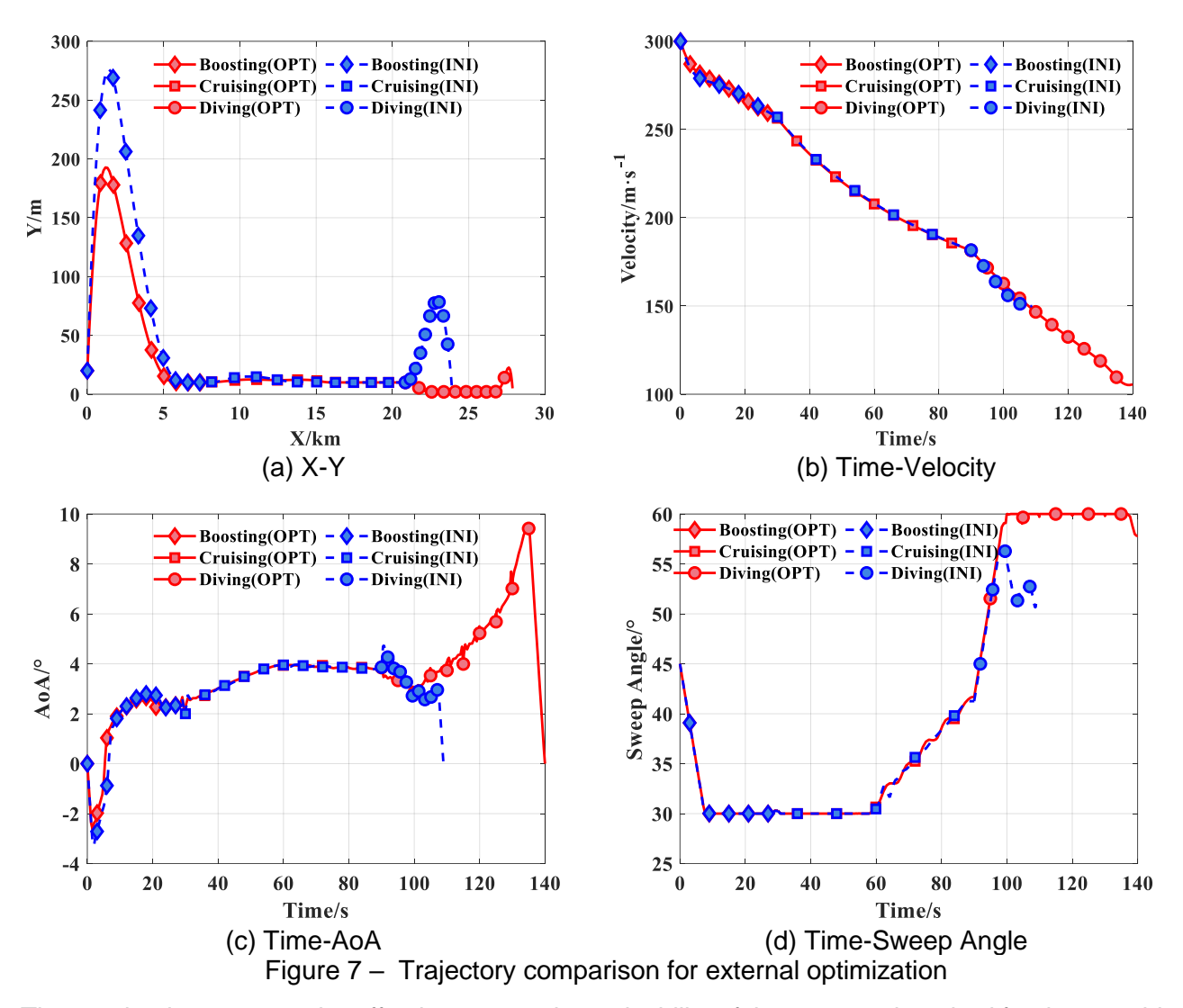
4.3 External Optimization Result and Analysis

After external optimization, the results are summarized in Table 3 and Figure 7. From Table 3 and Figure 7, it can be found that $\theta_{AB,0}$ is decreased to gain a longer flight range of the boosting phase.

The optimized values of $\theta_{\text{BC},0}$ and $\theta_{\text{CD},0}$ are close to the initial ones, since the flight altitude reaches the predefined boundary (i.e., 10~20m) in the cursing phase. As for the diving phase, the final velocity is decreased to the low boundary of the design space, where more kinetic energy can be saved to extend the flight time. In this way, the optimized solution generates a 15.86% improvement in the total range.

Table 3 - Comparison of optimized and initial results

rable of Companion of Spanies and make receive								
Category	Parameter	Symbol	Unit	Initial	Optimized			
Objective	Total trajectory	$R_{ m total}$	km	24.0565	27.8711			
Design	Initial trajectory angle in boosting	$ heta_{ ext{AB},0}$	0	20.0000	15.5049			
	Initial trajectory angle in cruising	$ heta_{ ext{BC},0}$	0	0	0.0114			
	Initial trajectory angle in diving	$ heta_{ ext{CD},0}$	0	0	-0.0478			
	Final trajectory angle in diving	$ heta_{ ext{CD,f}}$	0	-10.0000	-9.1552			
	Final velocity	$V_{ m CD,f}$	m/s	150.0000	105.6720			



The results demonstrate the effectiveness and practicability of the proposed method for the morphing flight vehicle performance improvement.

5. Conclusion

To improve the trajectory performance for the morphing flight vehicles, this paper proposes a surrogate-assisted hierarchical optimization method, consisting of inner and external optimization processes. After inner optimization process, the optimal control variables, i.e., angles of attack and sweep angles, for each trajectory phase can be obtained. The total flight range can be improved by 6.79% compared with the fixed wing. Furthermore, the external optimization process refines the boundary states of different phases and is solved by a kriging surrogate-assisted differential evolution. In the external optimization, a 15.86% improvement is achieved for the flight range.

In future work, the different morphing modes, i.e., variable camber and span wings, are required to be investigated to reveal the morphing influence on the trajectory performance. Additionally, the entire aerial-aquatic trajectory optimization is considered to be our next work.

6. Contact Author Email Address

The contact author is Prof. Renhe Shi. The corresponding email is srenhe@163.com.

7. Copyright Statement

The authors confirm that they and their organization, hold copyright on all of the original material included in this paper. The authors also confirm that they have obtained permission, from the copyright holder of any third party material included in this paper, to publish it as part of their paper. The authors confirm that they give permission, or have obtained permission from the copyright holder of this paper, for the publication and distribution of this paper as part of the ICAS proceedings or as

individual off-prints from the proceedings.

Acknowledgments

This study was co-supported by the National Natural Science Foundation of China (Grant Nos. 92371101, 52272360, and 52232014), Beijing Natural Science Foundation (Grant No. 3222019), Chongqing Natural Science Foundation (CSTB2023NSCQ-MSX0300), Beijing Institute of Technology Research Fund Program for Young Scholars (Grant No. XSQD-202101006), and BIT Research and Innovation Promoting Project (Grant No. 2022YCXZ017).

References

- [1] Chen X, Li C, Gong C, Gu L and Ronch AD. A study of morphing aircraft on morphing rules along trajectory. *Chinese Journal of Aeronautics*, Vol. 34, No. 7, pp 232-243, 2021.
- [2] Dai P, Yan B, Huang W, Zhen Y, Wang M and Liu S. Design and aerodynamic performance analysis of a variable-sweep-wing morphing waverider. *Aerospace Science and Technology*, Vol. 98, p 105703, 2020.
- [3] Ajaj RM, Beaverstock CS and Friswell MI. Morphing aircraft: The need for a new design philosophy. *Aerospace Science and Technology*, Vol. 49, pp 154-166, 2016.
- [4] Yuan G, Gu L and Pan L. Modeling and simulating dynamics of missiles with deflectable nose control. *Chinese Journal of Aeronautics*, Vol. 22, No. 5, pp 474-479, 2009.
- [5] Zhang Z, Tang Q, Sun X and Chen Z. Trajectory optimization of a deflectable nose missile. *Defence Technology*, Vol. 13, No. 3, pp 158-163, 2017.
- [6] Munroe E, Bohrer R, Chishty WA and Kim IY. Structural design of a morphing serpentine inlet using a multi-material topology optimization methodology. *Structural and Multidisciplinary Optimization*, Vol. 64, No. 1, pp 389-422, 2021.
- [7] Collis SS, Joslin RD, Seifert A and Theofilis V. Issues in active flow control: theory, control, simulation, and experiment. *Progress in Aerospace Sciences*, Vol. 40, No. 4, pp 237-289, 2004.
- [8] Chu L, Li Q, Gu F, Du X, He Y and Deng Y. Design, modeling, and control of morphing aircraft: A review. Chinese Journal of Aeronautics, Vol. 35, No. 5, pp 220-246, 2022.
- [9] Li D, Zhao S, Da Ronch A, Xiang J, Drofelnik J, Li Y, Zhang L, Wu Y, Kintscher M, Monner HP, Rudenko A, Guo S, Yin W, Kirn J, Storm S and Breuker RD. A review of modelling and analysis of morphing wings. *Progress in Aerospace Sciences*, Vol. 100, pp 46-62, 2018.
- [10]Zhang X, Xie C, Liu S, Yan M and Xing S. Development needs and difficulty analysis for smart morphing aircraft. *Acta Aeronautica et Astronautica Sinica*, Vol. 44, No. 21, p 529302, 2023.
- [11] Vos R and Farokhi S. *Aerodynamics of swept wings, introduction to transonic aerodynamics*. Springer Netherlands, Dordrecht, 2015.
- [12]Bae JS, Seigler TM and Inman DJ. Aerodynamic and Static Aeroelastic Characteristics of a Variable-Span Morphing Wing. *Journal of Aircraft*, Vol. 42, No. 2, pp 528-534, 2005.
- [13]Lyu J, Dong Y and Chen Y. Rules of the optimal variable sweep wing in low and medium height. *Flight Dynamics*, Vol. 34, No. 2, pp 24-27, 2016.
- [14]Malyuta D, Yu Y, Elango P and Açıkmeşe B. Advances in trajectory optimization for space vehicle control. *Annual Reviews in Control*, Vol. 52, pp 282-315, 2021.
- [15]Chai R, Chen K, Cui L, Chai S, Inalhan G and Tsourdos A. Review of Advanced Trajectory Optimization Methods, Advanced Trajectory Optimization, Guidance and Control Strategies for Aerospace Vehicles: Methods and Applications. Springer Nature Singapore, Singapore, 2023.
- [16]Dai P, Yan B, Liu R, Liu S and Wang M. Integrated Morphing Strategy and Trajectory Optimization of a Morphing Waverider and Its Online Implementation Based on the Neural Network. *IEEE Access*, Vol. 9, pp 59383-59393, 2021.
- [17]Gong C, Zhu Z, Chen B, Su H and Gu L. Bi-Level Global Optimization Method for Multi-Branching Trajectory. Journal of Astronautics, Vol.38, No. 9, pp 903-910, 2017.
- [18]Wu Y, Deng J, Li L, Su X and Lin L. A hybrid particle swarm optimization-gauss pseudo method for reentry trajectory optimization of hypersonic vehicle with navigation information model. *Aerospace Science and Technology*, Vol. 118, p. 107046, 2021.
- [19]Brunton SL, Nathan Kutz J, Manohar K, Aravkin AY, Morgansen K, Klemisch J, Goebel N, Buttrick J, Poskin J, Blom-Schieber AW, Hogan T and McDonald D. Data-Driven Aerospace Engineering: Reframing the Industry with Machine Learning. *AIAA Journal*, Vol. 59, No. 8, pp 2820-2847, 2021.
- [20] Viana FAC, Gogu C and Goel T. Surrogate modeling: tricks that endured the test of time and some recent developments. *Structural and Multidisciplinary Optimization*, Vol. 64, pp 2881-2908, 2021.
- [21]Ye N, Long T, Meng J, Shi R and Zhang B. Surrogate-assisted optimization for anti-ship missile body configuration considering high-velocity water touching. *Chinese Journal of Aeronautics*, Vol. 36, No. 12, pp 268-281, 2023.

INSERT RUNNING TITLE HERE

- [22]Ruan S and Ma Y. Optimization of acceleration motion trajectory of SHEV based on radau pseudospectral method. *IFAC-PapersOnLine*, Vol. 52, No. 5, pp 48-53, 2019.
- [23]Sun Y, Meng X, Long T and Wu Y. A fast optimal Latin hypercube design method using an improved translational propagation algorithm. *Engineering Optimization*, Vol. 52, No. 7, pp 1244-1260, 2020.
- [24] Deb K. An efficient constraint handling method for genetic algorithms. *Computer Methods in Applied Mechanics and Engineering*, Vol. 186, No. 2, pp 311-338, 2000.
- [25]Opara KR and Arabas J. Differential Evolution: A survey of theoretical analyses. *Swarm and Evolutionary Computation*, Vol. 44, pp 546-558, 2019.